ADVANCES IN ATMOSPHERIC SCIENCES, VOL. 21, NO. 5, 2004, 675–690

An Eddy-Permitting Oceanic General Circulation Model and Its Preliminary Evaluation

LIU Hailong* (刘海龙), ZHANG Xuehong (张学洪), LI Wei (李 薇),
YU Yongqiang (俞永强), and YU Rucong (宇如聪)

State Key Laboratory of Numerical Modeling for Atmospheric Sciences and Geophysical Fluid Dynamics, Institute of Atmospheric Physics, Chinese Academy of Sciences, Beijing 100029

(Received 15 January 2004; revised 19 March 2004)

ABSTRACT

An eddy-permitting, quasi-global oceanic general circulation model, LICOM (LASG/IAP (State Key Laboratory of Numerical Modeling for Atmospheric Sciences and Geophysical Fluid Dynamics, Institute of Atmospheric Physics) Climate System Ocean Model), with a uniform grid of $0.5^\circ \times 0.5^\circ$ is established. Forced by wind stresses from Hellerman and Rosenstain (1983), a 40-yr integration is conducted with sea surface temperature and salinity being restored to the Levitus 94 datasets. The evaluation of the annual mean climatology of the LICOM control run shows that the large-scale circulation can be well reproduced. A comparison between the LICOM control run and a parallel integration of L30T63, which has the same framework but a coarse resolution, is also made to confirm the impact of resolution on the model performance. On account of the reduction of horizontal viscosity with the enhancement of the horizontal resolution, LICOM improves the simulation with respect to not only the intensity of the large scale circulations, but also the magnitude and structure of the Equatorial Undercurrent and South Equatorial Current. Taking advantage of the fine grid size, the pathway of the Indonesian Throughflow (ITF) is better represented in LICOM than in L30T63. The transport of ITF in LICOM is more convergent in the upper layer. As a consequence, the Indian Ocean tends to get warmer in LICOM. The poleward heat transports for both the global and individual basins are also significantly improved in LICOM. A decomposed analysis indicates that the transport due to the barotropic gyre, which primarily stands for the barotropic effect of the western boundary currents, plays a crucial role in making the difference.

Key words: eddy-permitting, oceanic general circulation model, large-scale circulation

1. Introduction

The current oceanic general circulation models (GCMs) used in climate studies, especially those serving as component models in coupled GCMs, have an average resolution around 2° (IPCC, 2001). The oceanic GCMs with relatively coarse resolutions can reproduce the major observed features of the large-scale circulations, but there are some insurmountable difficulties. It was documented by Gates (1992) that the main defects of the coarse resolution oceanic GCMs include the representation of realistic geometry and bathymetry, the dependence on the parameterization of the convective, mixing, and meso-scale eddy processes, the distortion of western boundary currents and upper ocean circulation, etc. These deficiencies have important influences on the modeled climate system, resulting in a weak meridional heat transport, lack of real western boundary currents, or a weak Equatorial Undercurrent (EUC), which limits the simulation ability of the whole climate system model.

The choice of a high resolution, regional oceanic model is usually for the sake of economical computation. It is, however, not fully appropriate to the simulation of the general oceanic circulation due to its global scale, including such elements as the thermohaline circulation and the Antarctic Circumpolar Circulation (ACC). The difficulty in determining the boundary conditions is also an obstacle.

The establishment of high resolution oceanic GCMs began in the late 1980s. There have been

*E-mail: lhl@lasg.iap.ac.cn

three representative models, including the Semtner and Chervin model (Semtner and Chervin, 1988; refered to as the SC model hereafter), the Parallel Ocean Climate Model (POCM, Fu and Smith, 1996), which is the latest version of the SC model, and the Los Alamos National Laboratory (LANL) Parallel Ocean Program model (POP, Smith et al., 1992), which is designed to run on a parallel-processor computer. The applications of high resolution models improve our understanding of the ocean circulation. For instance, the results of the SC model gave support to the assumption of the warm water routine in the thermohaline circulation theory (Semtner and Chervin, 1992; SC92 hereafter). Limited by the groundwork and computation conditions as well, the studies of high resolution oceanic GCMs in China have lagged behind the international community, and results were not published until the late 1990s. Based on MOM2 (Pacanowski, 1995), for instance, a global GCM ($1^\circ \times 1^\circ$) with a zoomed grid $[(1/3)^\circ \times (1/3)^\circ]$ in the North Pacific was configured by Wei (1999) to investigate the marginal seas of China.

There have been three generations of oceanic GCMs developed in LASG/IAP (State Key Laboratory of Numerical Modeling for Atmospheric Sciences and Geophysical Fluid Dynamics, Institute of Atmospheric Physics) since the late 1980s. Each of them served as a component model of a climate system model in LASG. In examining the course of the evolution of the models (Table 1), the increase of the spatial resolutions in both horizontal and vertical directions is regarded as a landmark. Estimates of the third generation model, which has a grid size of about $1.875^\circ \times 1.875^\circ$ following a T63 resolution in the atmospheric GCM and 30 layers in the vertical (hence the name L30T63), showed an evident improvement compared to the second generation with regard to the simulation of the main thermocline, thermohaline circulation, and meridional heat transport (Jin et al., 1999; JZZ99 hereafter). It was also revealed that some model errors are related to the coarse resolution it employed. The lessened strength of the North Equatorial Countercurrent (NECC) and EUC, and the enhanced strength and greater depth of the South Equatorial Current (SEC) at the equator, were both at least partly ascribed to the coarse grid in the meridional direction (Jin et al., 2000). There is no doubt that a higher resolution is a chief step in the development of L30T63.

In the present study, an eddy-permitting quasi-global model with a uniform grid of $0.5^\circ \times 0.5^\circ$ was established based on L30T63. The size of 0.5° is a marginal resolution to resolve the first-baroclinic Rossby radius of deformation at the equator, though it is not fine enough to resolve the meso-scale eddies (Philander, 1990). The value is also a required resolution to represent the complicated topography within the Indonesian Sea (Fig. 1a). In the vertical, 30 layers are kept those in L30T63. The high resolution version of the third generation model is named "LICOM" (LASG/IAP Climate System Ocean Model). The current version is 1.0, and hereafter, it is referred to as "LICOM" instead of "LICOM1.0" for simplicity.

The present study aims at a basic estimate of the annual mean climatology of LICOM and a verification of the effect of enhanced resolution on the ocean modeling with respect to the large-scale circulation, meridional heat transport, upper circulation in the tropical Pacific, and the Indonesian Throughflow (ITF). The work is organized into six sections. The second section describes the model and experiments. The simulation of the annual mean climatology follows in the third section. The comparisons of simulated circulations and thermal conditions between the high and coarse resolutions models are shown in the fourth and fifth sections, respectively. The last section gives the summary and discussions.

Table 1. The development of the IAP/LASG global oceanic general circulation model.

Version	Resolution	Scope	References	Coupled model
First generation	$5^\circ \times 4^\circ$, 4 layers	60°S–60°N	Zhang and Liang, 1989	Coupled with IAP two-layer AGCM (Zeng et al., 1989) Zhang et al., 1992
Second generation	$5^\circ \times 4^\circ$, 20 layers	global	Zhang et al., 1996	Coupled with IAP two-layer AGCM (Zeng et al., 1989), Chen, 1994 and IAP 9-layer, R15 spectral AGCM (Wu et al., 1996). Liu et al., 1996; Yu, 1997; Wu et al., 1997; Yu and Zhang, 1998
Third generation (L30T63)	T63 (approx. $1.875^\circ \times 1.875^\circ$), 30 layers	global	Jin et al., 1999	Coupled with a T63 spectral AGCM (Dong et al., 2000), Yu et al., 2000; Liu, 2001 and CCM3 (Kiehl, 1998), Yu et al., 2002

Table 2. LICOM (control run) and L30T63 (experiment D2, see JZZ99).

	LICOM	L30T63
Horizontal Resolution	0.5°	1.875°
Horizontal Viscosity	5×10^3 m^2 s^{-1}	2×10^5 m^2 s^{-1}
Model Domain	75°S–65°N	global
Bathymetric Data	DBDB5(1/12°)	Scripps (1°)
Boundary Condition	Restoring, 30 days for thermal and 90 days for salinity	Haney type (Haney, 1971) for thermal, and restoring for salinity (90 days)
Dataset	Sea surface temperature and salinity from Levitus 94	COADS dataset (da Silva et al., 1994) and sea surface salinity from Levitus 94

2. The model and experiments

Free surface primary equations, the corresponding energy conserving numerical differential scheme, and the η-coordinate in the vertical are the primary features of the framework of LASG/IAP oceanic GCMs and they have been maintained in LICOM (Liu, 2002). Some sophisticated parameterization schemes, including the Gent and McWilliams (1990) parameterization of meso-scale eddies and the Richardson-number dependent mixing process (Pacanowski and Philander, 1981), which were introduced in L30T63 and led to some notable improvement in the simulation of the permanent thermocline, thermohaline circulation, and meridional heat flux, are also included in LICOM. See JZZ99 for more details of the fundamental framework and performance of L30T63.

The chief differences between the control run of LICOM and experiment D2 of L30T63 (JZZ99) are listed in Table 2. The number of total gridpoints increases by a factor of 14 when the resolution is enhanced from T63 to 0.5°.

2.1 *Model domain*

The convergence of the meridians at the poles in the spherical coordinate system leads to a numerical instability with the CFL (Cowarant, Friedrics and Lewy) condition. Therefore, most of the high resolution global oceanic GCMs exclude the polar area in their early stages. The model domain is chosen to be between 75°S and 65°N in the present study. The Bering Strait is closed, and there is no exchange between the Arctic Ocean and the North Atlantic. The lateral boundary conditions at high latitudes are set to be rigid for the velocity, and non-flux for the tracers, except for the northern and southern boundaries. To avoid a long-term climate drift, a 120-day restoring timescale is adopted within 10° of the southern and northern walls as in Semtner and Chervin (1992). The thermodynamic dynamic sea ice model used in L30T63 is no longer necessary in the current experiments of LICOM. Sea surface temperatures (SSTs) that are less than –1.8°C are simply restored to –1.8°C.

2.2 *Model topography*

The model topography is derived from the Digital Bathymetric Data Base 5 minute (DBDB5) of the Naval Oceanographic Office. The topography data were first averaged onto a horizontal grid of (1/3)° and then interpolated onto the (1/2)° grid. Some main straits, such as the Strait of Gibraltar, Tsushima Strait, Soya Strait, Luzon Strait, Taiwan Strait, and Torres Strait, are open in the model. In the Arakawa B-grid scheme, an "open" passage means there are at least two rows of grids. The Baltic Sea, Black Sea, Caspian Sea, Red Sea, Persian Gulf, and Hudson Bay were filled manually. This is called the topography-1 of LICOM.

The main pathways of ITF, including the Makassar Strait, Lombok Strait, Ombai Strait, and Timor Passage, are able to be represented in the topography-1. A further comparison with the original bathymetric data, however, reveals some problems. The Karimata and Torres Straits are much deeper than in reality because the water columns are required to have at least 5 levels (125 m) in the model. Additionally, the narrow channel at the south end of the Makassar Strait is not resolved by the $0.5^\circ \times 0.5^\circ$ grid, which makes the Makassar Strait shallower than in reality. As a result, the volume transports are chiefly through the Karimata and Torres Straits (–5.2 Sv and –6.8 Sv respectively for the integration based on the topography-1) (1 Sv=10^6 m^3 s^{-1}) rather than the Makassar Strait (–0.8 Sv), which is the dominant ITF pathway in the Indonesian Sea in reality. Alterations were made by hand to narrow and shallow the Karimata and Torres Straits and to deepen the Makassar Strait as well, which is called topography-2 of LICOM (Fig .1a). As a comparison, the water is transferred from the Pacific Ocean into the Indian Ocean through the widened passages both between Sulawesi and New Guinea and be-

tween Sumatra and Kalimantan in L30T63 (Fig. 1b).

2.3 *Horizontal viscosity*

The horizontal viscosity should be reduced as the horizontal resolution is enhanced. According to the configuration of other high-resolution models (Stockdale et al., 1993), the horizontal viscosity is set to be 5×10^3 m^2 s^{-1} between 50°N and 50°S (1×10^4 m^2 s^{-1} for the first 10 years of integration). A larger horizontal viscosity (2×10^4 m^2 s^{-1}) is used at high latitudes.

2.4 *Experiments*

A restoring surface boundary condition is employed with the restoring coefficients for SST and sea surface salinity (SSS) being set to 30 days and 90 days, respectively. The observed SST and SSS are both from the Levitus 94 datasets (Levitus and Boyer, 1994; Levitus et al., 1994). Hellerman and Rosenstein wind stresses (Hellerman and Rosenstein, 1983) are adopted with a reduction between 30°N and 30°S, which was suggested by Stockdale et al. (1993).

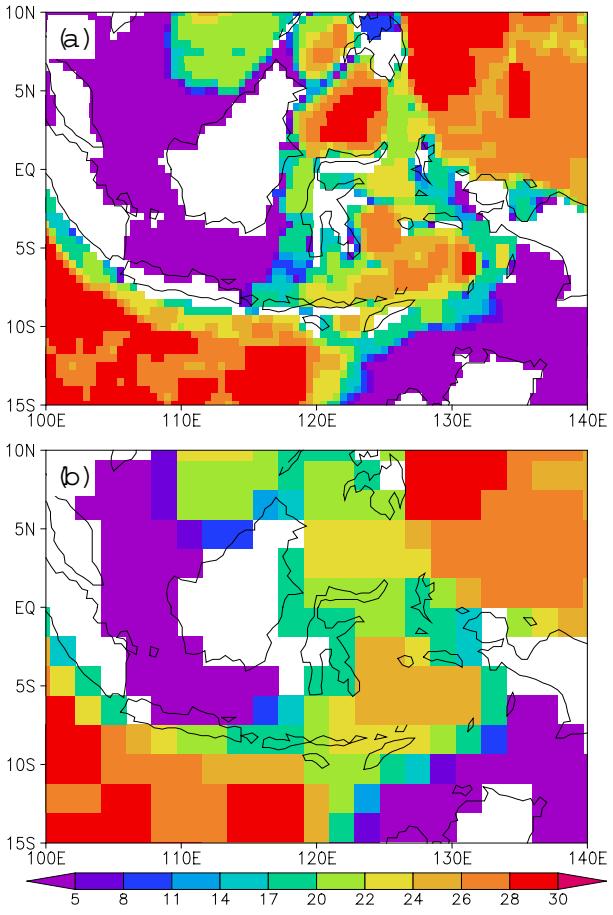

Fig. 1. The model topography of LICOM (a) and L30T63 (b). The color denotes the number of model levels.

The control run was initialized with the three-dimensional distribution of salinity and temperature from Levitus 94 and from a motionless state. Annual mean and monthly climatology of wind stresses from Hellerman and Rosenstein (1983) served as the forcings for the first and second 20 years of the control run, respectively. The topography-1 was used in the 40-yr control run integration. The annual mean of the previous year's control run is examined for the model climatology. An additional three 3 years of integration is conducted from the end of the LICOM control run when topography-2 is used instead of the topography-1.

A parallel experiment was conducted employing L30T63 with the same configuration as LICOM, expect that the horizontal viscosity was set to 5×10^4 m^2 s^{-1} between 50°N and 50°S. The 40th year's annual mean results of L30T63 are compared with those from the LICOM control run except in section 4.3, where the 43rd year LICOM integration is used to examine the modeled ITF.

3. Model climatology

3.1 *Global averaged kinetic energy, SST, and sea temperature*

The daily global mean kinetic energy is presented in Fig. 2a. Since most kinetic energy lies in the upper layer, the model approaches its dynamic equilibrium after 10 years of integration. SST reaches a stable state as soon as the kinetic energy does (Fig. 2b). The global mean potential temperature, however, shows a slight, long-term cooling drift (Fig. 2c). A similar long term drift is detected for the global mean salinity (towards freshness; figure omitted). Due to the restoring boundary condition used in the present study, the simulated SST and SSS resemble the observation very much, though the sea surface heat and the freshwater fluxes are relatively poorly reproduced. The biases in the surface fluxes, in turn, lead to the errors of the temperature and salinity beneath the surface and result in the drift of temperature and salinity. For the mixing processes involved, the timescale of the model adjustment is as long as millennia. This is why an oceanic GCM needs thousands of years of integration to approach equilibrium.

3.2 *Zonal mean potential temperature and salinity*

Figure 3a shows the modeled zonal mean potential temperature and its differences from Levitus 94. Because of the introduction of meso-scale eddies parameterization of Gent and McWilliams (1990), the model-

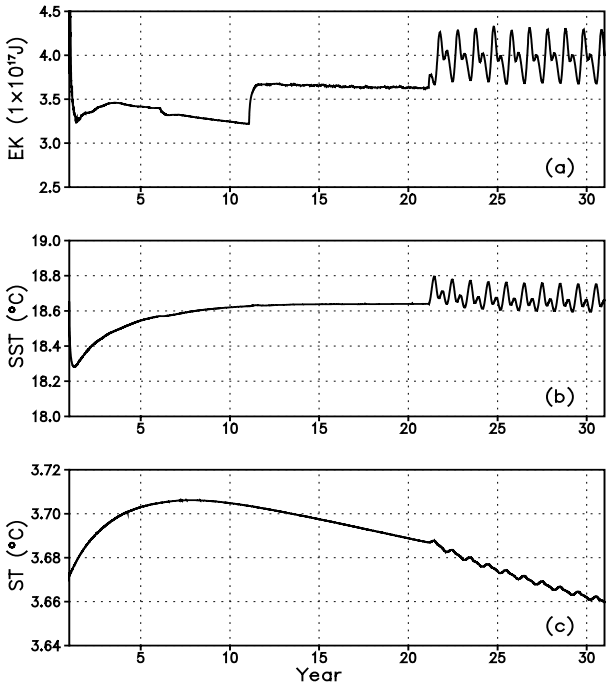

Fig. 2. The global mean kinetic energy (a, 1×10^{17} J), SST (b, °C), and sea temperature (c, °C) of LICOM.

ed permanent thermocline, which is often represented by the 4°C isotherm, is located just below 1000 m. This is consistent with the observation. Comparison between LICOM results and Levitus 94 data shows that the evident errors of potential temperature appear within the upper 600 m. The difference is less than 1°C below that depth. The maximum bias exceeding 5°C lies at 40°N, and between 100 m and 200 m. It is apparent that the discrepancies arise primarily from the western part of the basin (figure omitted). The large errors in potential temperature result from both the inaccuracy of surface forcing and the unreal western boundary currents simulated by LICOM. Below 600 m, the simulation is colder than the observation between 40°S and 50°N and warmer at higher latitudes. The cold bias in the deep ocean is compatible with the cooling trend of the global mean potential temperature (Fig. 2c), suggesting the adjustment in the deep ocean is still in process.

The zonal mean salinity is presented in Fig. 3b. Both the high salinity centers in the subtropics and the northward-spreading Antarctic Intermediate Water (AIW) are still maintained. The major bias of salinity also occurs in the upper layer (above 400 m). The salinity is lower than Levitus 94 between 40°S and 40°N, and higher in the poleward regions. Positive biases are evident in the western basin, while negative biases are in the east (figure omitted).

3.3 *Horizontal general circulation*

Figure 4a gives the barotropic stream function (BSF). BSF reflects the vertically integrated horizontal circulation in which SEC, the North Equatorial Current (NEC), NECC, and EUC are all reproduced in the tropical Pacific Ocean. The magnitude of the recirculation consisting of NEC, the Mindanao Current (MC), and NECC exceeds 30 Sv.

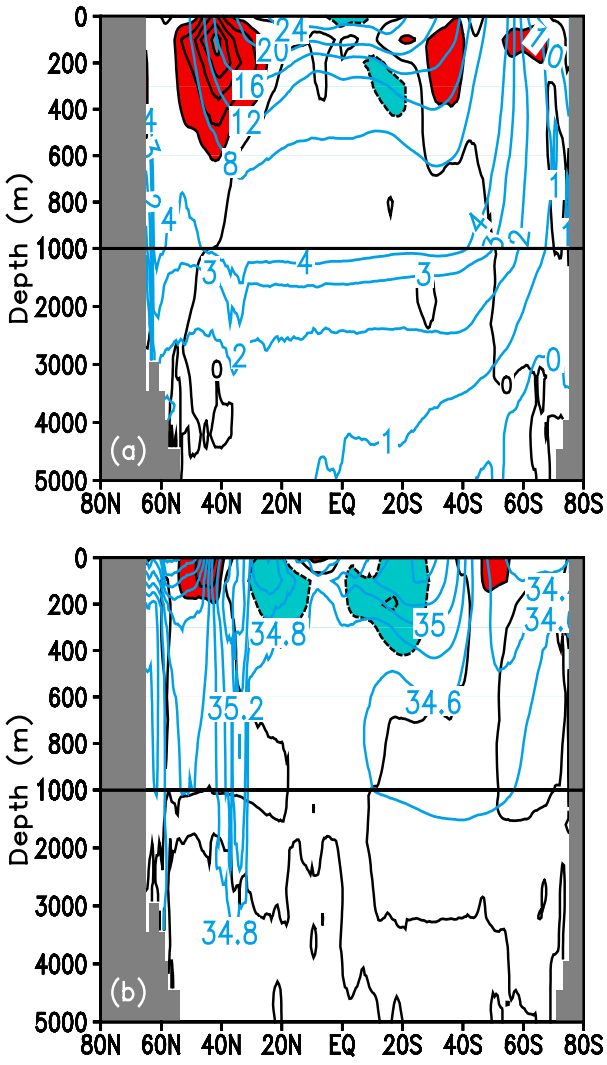

Fig. 3. The LICOM simulated zonal mean temperature (a) and salinity (b) (light contours) and their differences from Levitus 94 (dark contours). The differences are contoured at intervals of 1°C or 0.2 psu, with shading where the absolute values exceed 1°C or 0.2 psu.

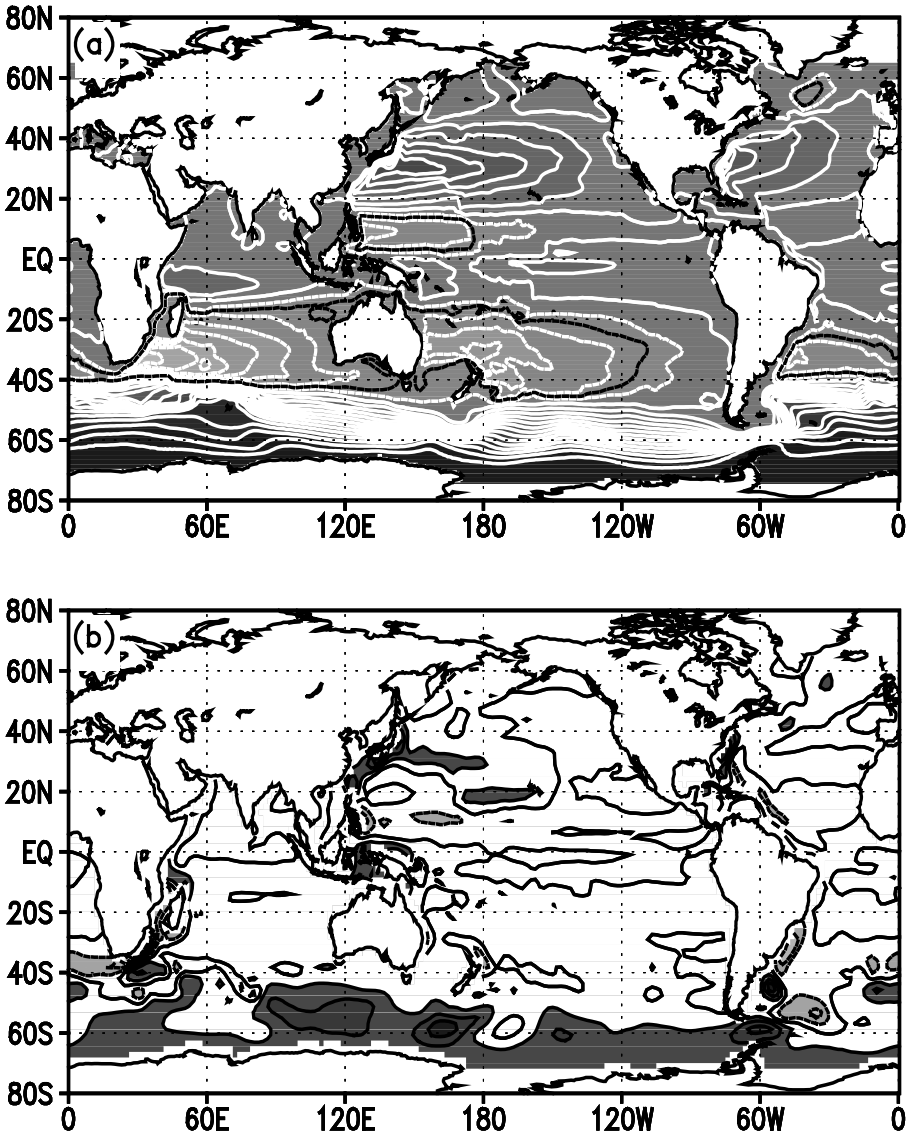

Fig. 4. (a) The LICOM-simulated barotropic stream function. The contour interval is 10 Sv (1 Sv=10^6 m^3 s^{-1}) where 15 Sv is denoted by a thick line. (b) The differences of the simulated barotropic stream function between LICOM and L30T63. The interval is 5 Sv with shading where the absolute values exceed 5 Sv.

The subtropical gyres in the Northern Hemisphere are characterized by the strong western boundary currents closed by the slow and broad currents in the eastern basin. The modeled Kuroshio and Gulf Stream reach 60 Sv and 40 Sv, respectively, which are compatible with the results of SC92 (their Fig. 10). In contrast to the Northern Hemisphere, the subtropical gyres in the Southern Hemisphere are linked up. The contour of 15 Sv passes Torres Strait and crosses the Indian Ocean. It then enters the Atlantic Ocean around the southern tip of Africa and joins the ACC. Eventually, it goes back to the Pacific Ocean through the strait between Australia and Tasmania. The 15 Sv transport of BSF comes mostly from the ITF transport in LICOM. The magnitude of BSF coincides with the results of the theory of Island Rule (Godfrey, 1989, 1996) but not its routes, in which the ITF wanders its way through the Indonesian Sea instead of the Torres Strait.

The subpolar gyres in the Northern Hemisplere are wholly weak compared with SC92. The strongest one that is in the Atlantic Ocean is only 15 Sv. The magnitude of ACC in the Southern Hemisphere is 130 Sv, which is close to the observation (118–146 Sv, Whit-

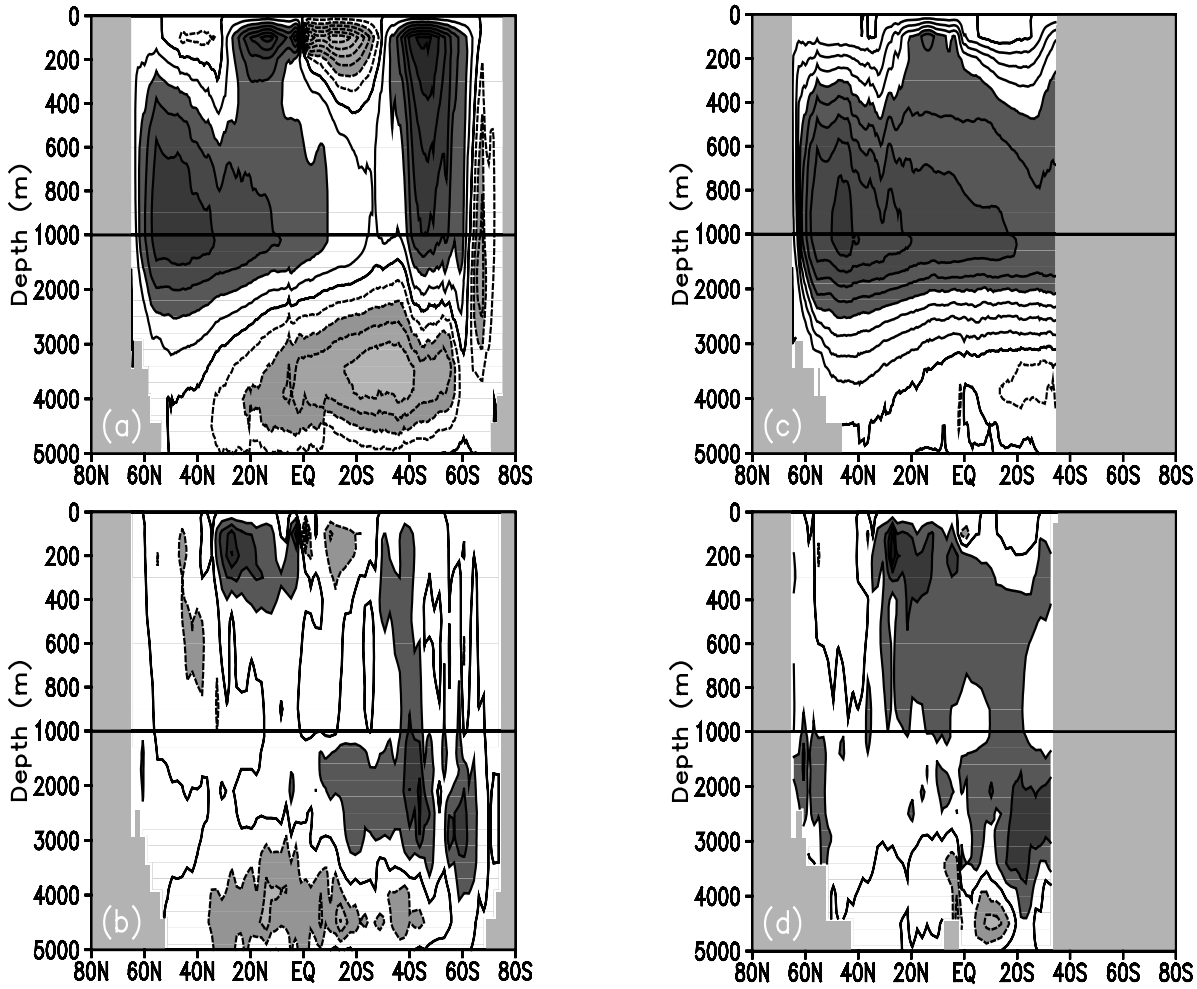

Fig. 5. (a) The LICOM-simulated meridional stream function and (b) the difference between LICOM and L30T63 for the global ocean. (c) as (a) but for the Atlantic Ocean. (d) as (b) but for the Atlantic Ocean. Countour intervals are (a) 4 Sv, (b) 2 Sv, (c) 2 Sv, (d) 1 Sv.

worth, 1983).

3.4 *Meridional overturning circulations*

The large scale oceanic general circulation is more complicated in three-dimensional structure than we image. The meridional overturning stream function (MSF), i.e., the zonal integration of the volume transport within a basin, is a simplification of the meridional circulation and also a common way to present the thermohaline circulation. Figures 5a and 5c show the MSFs for the global ocean and the Atlantic Ocean, respectively. In the upper layer, the intense upwelling at the equator and downwelling around 30° of both hemispheres constitute the Ekman cells (Fig. 5a). There is no corresponding closed cell in the Atlantic Ocean (Fig. 5c), which suggests that the Ekman cells found in Fig. 5a mainly exist in the Pacific and Indian Oceans. The Deacon Cell in the South Ocean, which combines the effects of wind, buoyancy, and topography, penetrates much deeper than the Ekman cells. The contour of 4 Sv in the Deacon Cell can reach more than 2000 m. In the subsurface, the large cell centered at 800 m primarily stands for the thermohaline circulation of the North Atlantic Ocean. The maximum transport of North Atlantic Deep Water (NADW) is 16 Sv and the transport at the southern end is approximately 10 Sv (Fig. 5c). Because of the incomplete adjustment in the deep ocean, the Antarctic Bottom Water (AABW) in LICOM is too strong (16 Sv) compared with the results of L30T63 (JZZ99, Fig. 8). Furthermore, AABW occurs mainly in the Indo-Pacific Ocean, ascribed partly to the coarse vertical resolution in the deep ocean.

Comparing the simulated MSF with that of SC92, we find two aspects of the differences. First, the upwelling in the deep ocean is much stronger in SC92 than in LICOM. Second, NADW simulated by SC92

is weaker than that in LICOM. These are probably due to the robust diagnostic technology in the deep ocean employed in SC92.

4. Effects of horizontal resolution on the simulation of circulation

With the enhancement of the horizontal resolution, more physical processes can be explicitly expressed which leads to less dependence on sub-grid parameterizations (Griffies et al., 2000). The horizontal viscosity is reduced accordingly. In this section, the primary changes of the large-scale circulation caused by the enhancement of the horizontal resolution have been assessed.

4.1 *Large scale general circulation*

Figure 4b shows the differences of BSF between LICOM and L30T63. Some distinct discrepancies can be found for the western boundary currents, especially the Kuroshio and its extension, the Mozambique Current, the Agulhas Current and its recirculation, and the Brazil Current. The western boundary currents in LICOM are stronger in intensity and closer to the boundary than those in L30T63. The ACC is more intensified in LICOM, which is accompanied by the enhanced meridional gradient of SST and sea surface height (SSH) (figure omitted). The NEC, NECC, and MC in LICOM are all stronger than those in L30T63 for more water is lost through the ITF passage in L30T63.

Almost each component of the meridional overturning circulation is reinforced in LICOM. For the global ocean (Fig. 5b), the magnitude of Ekman cell transport in LICOM is greater than that in L30T63 for both hemispheres. Not only the magnitude but also the penetrating depth of the Deacon Cell is greater in the LICOM simulation. The Deacon Cell extends to 3000 m in LICOM, while it is confined to around 2000 m in L30T63. The AABW in LICOM is also much stronger, with a maximum difference of 4 Sv. In the Atlantic Ocean (Fig. 5d), it is evident that the wind driven upper layer circulation becomes stronger, as well as the cross equator transports of the intermediate and deep water.

4.2 *Tropical circulations*

The circulations in the tropical Pacific are sensitive to both the horizontal resolution and the viscosity. The white curves in Figs. 6a and 6b denote the zonal currents along 150°W. The main components of the tropical circulations are present, such as the SEC at the equator, the NECC between 5°N and 10°N, and the EUC just below the equator.

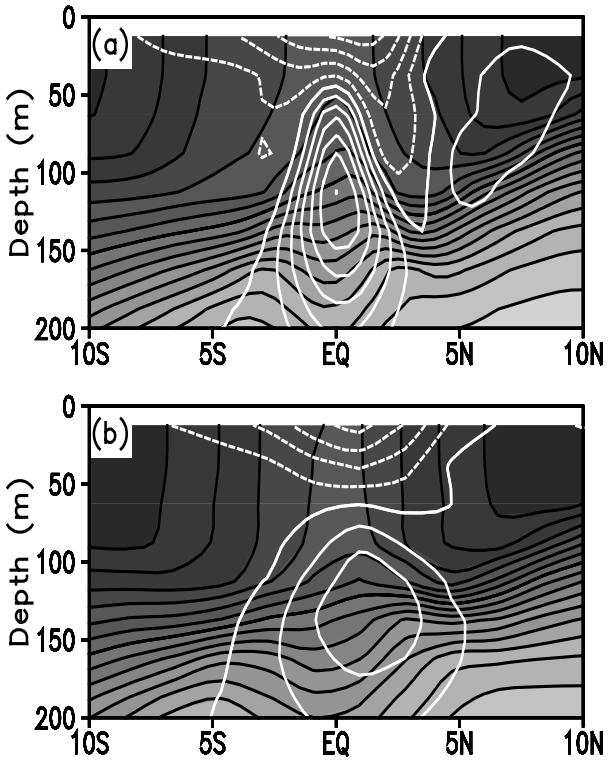

Fig. 6. The zonal current (white curves, interval of 0.1 m s^{-1}) and temperature (shaded, interval of 1°C with a thick curve for 20°C) along the 150°W depth-latitude section simulated by LICOM (a) and L30T63 (b).

The equatorial currents are better simulated in LICOM. The EUC in LICOM (0.6 m s^{-1}) is not only much stronger than that in L30T63 (0.2 m s^{-1}), but also much more convergent to the equator. The velocity of NECC reaches 0.1 m s^{-1} in LICOM, which is also larger than that in L30T63. Although the strengths of the simulated SEC in both models are almost equal (0.4 m s^{-1}), the structures are very different. The SEC confines itself on and around the equator in L30T63. In contrast, the LICOM-simulated SEC is shaped like a "W" with two centers separated on both sides of the equator. The secondary circulation in the upper equatorial Pacific Ocean is also intensified coinciding with the intensification of Ekman cells in MSF (figure not shown).

4.3 *ITF*

ITF is a system of currents within the Indonesian Sea which connect the Pacific Ocean and the Indian Ocean at low latitudes. It has been proved that ITF exerts significant influence over the global

climate in general and the tropical climate in particular (Hirst and Godfery, 1993; Schneider and Barnett, 1997; Scheider, 1998; Wajsowicz and Schneider, 2001). LICOM is capable of resolving the complex land-sea distribution within the Indonesian Sea, providing the precondition for a realistic simulation of ITF.

Figure 7 presents the upper 300 m averaged circulations within the Indonesian Sea simulated by LICOM and L30T63, respectively. In LICOM, the Makassar Strait is the primary passage of ITF. Passing the Sulawesi Sea, the majority of water from MC enters the Makassar Strait and exits the Indonesian Sea through the main gaps of the Less Sunda Islands, i.e., the Lombok Strait, Ombai Strait, and Timor Passage. Because of the obstruction of Halmahera Island, however, there is only a minor part of the currents off the New Guinea coast entering the Seram Sea through the passage east to Halmahera. Most of the water of the currents turns eastwards to join the EUC. The aforementioned characteristics of the simulated circulation agree well with the observations. Considerable transports are also

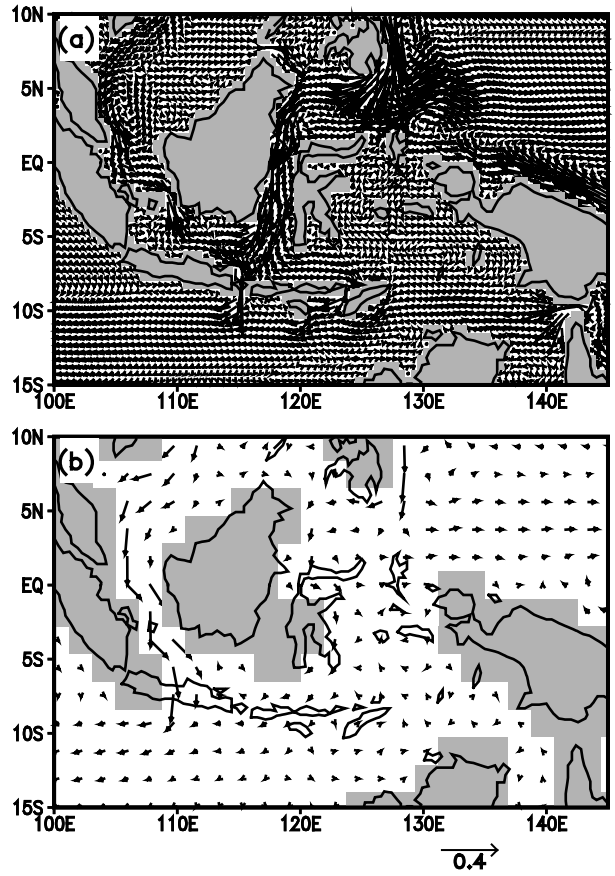

Fig. 7. The upper 300 m averaged currents around the Indonesian Seas from LICOM (a) and L30T63 (b).

produced through the Karimata Strait south of the South China Sea (SCS) and the Torres Strait between New Guinea and Australia. Although the exchanges between the Pacific and Indian Oceans through SCS have been yielded by other simulations (Masumoto and Yamagata, 1996; Lebdev and Yaremchuk, 2000, Fang et al., 2002), no observational evidence was given to support the pathway via SCS. The observed transport through the Torres Strait is also negligible (Wolanski et al., 1988).

The bathymetry of L30T63 in the Indonesian Sea is badly distorted and the width of the ITF passage exceeds 1000 km. The water from the Pacific Ocean and SCS flows directly into the Indian Ocean through the passage east to Sulawesi and west to Kalimantan.

Table 3 lists the volume transports of the primary passages within the Indonesian Sea. The total transport of ITF simulated by LICOM and L30T63 are 13.0 Sv and 17.8 Sv, respectively, which is comparable with the estimate using the "Island Rule" theory and within the range of the diversified observations (Godfrey, 1989, 1996). The Makassar Strait with a transport of –6.1 Sv is the main passage of ITF (see also Fig. 7). The value also agrees with the observation of Gordon et al. (1999). The secondary transport of ITF is via the eastern passages, by the Maluku Sea and Halmahera Sea, which is –4.4 Sv as a whole. There are only transports of –1.1 Sv and –1.4 Sv through the Karimata and Torres Straits, respectively.

In LICOM, a mass of water exits the Indonesian Sea through the Lombok (–3.9 Sv) and Ombai Straits (–7.0 Sv). Only a small part, –0.7 Sv, is through the Timor Passage. It is, however, not the case of the observation, in which only –1.7 Sv is found to pass through the Lombok Strait (Murray and Arief, 1988) while the Ombai Strait and Timor Passage comprise the main exits (Molcard et al., 1996; Molcard et al., 2001). The analogous imbalance in the distribution of transport between these straits is also seen in other oceanic models (Gordon and McClean, 1999).

Table 3 shows that although the total transport of ITF in L30T63 is 4.8 Sv larger than that in LICOM, the transports within the upper 440 m are almost equivalent. It is implied that ITF transport in LICOM is more concentrated in the upper layer, which is consistent with the observation and counted as one of the significant improvements of ITF simulation in LICOM.

Table 3. The simulated (LICOM and L30T63) and observed transports of the main passages within the Indonesian Sea (northwards and eastwards are positive, units: Sv).

	Total	Karimata	Makassar	M & H[a]	Torres	Lombok	Ombai	Timor
Observation	–12[b]	—	–9.3[c]	—	0.01[d]	–1.7[e]	–5[f]	–4.5[g] or –4.3[h]
LICOM	–13.0 (–9.7)[i]	–1.1	–6.1	–4.4	–1.4	–3.9	–7.0	–0.7
L30T63	–17.8 (–9.6)[i]	–6.3	—	–11.5	—	—	—	—

[a] M & H stands for the transport through both the Maluku Sea and Halmahera Sea
[b] the estimation of the geostrophic transports through the section between Australia and Sumatra using annual mean temperature and salinity from Levitus (Godfrey, 1989)
[c] the measurement in Makassar Strait around 3°S by a mooring buoy and averaged during 1997 (Gordon, 1999)
[d] from Wolanski et al. (1988)
[e] measured by current meter from January 1985 to March 1986 (Murray and Arief, 1988)
[f] measured by a single mooring buoy in 1995 (Molcard et al., 2001)
[g] the transport measured by current meter between 140 m and 1040 m in 1989 (Molcard et al., 1996)
[h] the transport measured by ADCP (Acoustic Doppler Current Profile) between 0 m to 1250 m in 1992 (Molcard et al., 1996)
[i] the value in parentheses is the transport within the upper 440 m

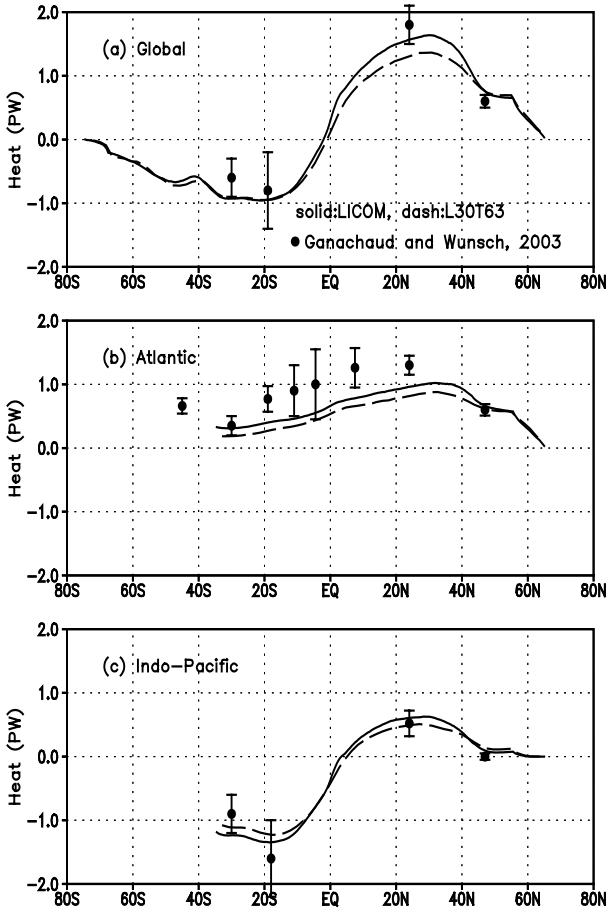

Fig. 8. The poleward heat transport for the global (a), the Atlantic (b), and the Indo-Pacific (c) Oceans simulated by LICOM (solid) and L30T63 (dashed) (units: PW) (1 PW=10^{15} W); the closed circles are the directed estimates from Ganachaud and Wunsch (2003).

5. Meridional heat transport (MHT) and thermal structure in the Indo-Pacific Ocean

With regards to climate research, ocean is of great importance in that it provides a significant portion of heat to the atmosphere. The changes in the structures of temperature and the heat transports are therefore essential aspects for the evaluation of an oceanic GCM.

5.1 *MHT*

Mesoscale eddy fluxes and boundary currents, which are considered to be important oceanic processes of heat transports, can be better resolved in the high resolution model than in the coarse one. Recently, two model studies have also shown an explicit dependence of ocean heat transport on resolution, ranging between 4° and 0.1° (Fanning and Weaver, 1997; Bryan and Smith, 1998). Although Gent et al. (1999) has pointed out that this dependence appears to be much weaker when more advanced sub-grid scale mixing parameterizations are used, the extent of the dependence of MHT on resolution is worth being evaluated.

Figure 8a shows that the enhanced general circulation in LICOM causes a large MHT. The evident difference between LICOM and L30T63 is located at about 30°N, where the maximum MHT also occurs. The value of the difference is 0.28 PW (1 PW=10^{15} W), as large as 1/5 of the maximum MHT. The results in the individual basins illustrate that the smaller difference in the Southern Hemisphere in Fig. 8a is due to the opposite sign of the model difference in the Atlantic Ocean and Indo-Pacific Ocean (Figs. 8b, c).

Also shown in Fig. 8 are the directed estimates of ocean heat transport from Ganachaud and Wunsch (2003) using a geostrophic inverse model and hydrographic sections obtained during WOCE (the World Ocean Circulation Experiment). In the Atlantic (Fig. 8b), the model heat transports are both approximately 0.5 PW smaller than that of the observation, except for at 47°N. LICOM is relatively close to the observation compared with L30T63. The small transport is usually a symptom of a meridional overturning in a model that is of insufficient size. In the Indo-Pacific basin (Fig. 8c), the heat transports in the models at four hydrographic sections are in agreement with the estimated value, either within or on the edge of the expected uncertainties. Such agreement may be taken to imply the quality of both the model circulation and the air-sea heat flux.

According to the formula of Fanning and Weaver (1997), the time averaged MHT due to the advection is decomposed into three terms: the baroclinic overturning, the barotropic gyre, and the baroclinic gyre. The baroclinic (barotropic) gyre represents the baroclinic (barotropic) part of the western boundary currents, while the baroclinic overturning is mainly for the Ekman cells.

The time mean term of MHT (Fig. 9a) strongly resembles the total one (Fig. 8a), suggesting that the enhancement of MHT does not result from the explicitly simulated eddies. Namely, the improvement in simulating eddies cannot lead to a significant increase of MHT. SC92 and Covey (1995) drew a similar conclusion from their studies.

The barotropic gyre components of MHT, which represent the structure of horizontal circulation (Fig. 4a), are nearly antisymmetric about the equator (Fig. 9b). The barotropic gyre term in LICOM is greater than that in L30T63 between 20°N and 40°N, a region occupied by the subtropical gyre (Fig. 4a). MHT due to the baroclinic overturning is caused by the combination of the Ekman transport and the transport of thermohaline circulation. It has signs opposite to those in the barotropic gyre term. The heat is transferred toward the equator at middle latitudes and toward the poles at both low and high latitudes (Fig. 9c). Thus, MHT contributed by the baroclinic overturning offsets part of that by the barotropic gyre at middle latitudes.

The discrepancy of MHT due to the baroclinic gyre is rather small between the two models. Therefore, the increase of MHT in LICOM is mainly caused by the barotropic circulation. This suggests that the western boundary currents play a key role in getting a realistic MHT, which was also pointed out by Wunsch (1996) and Covey (1995), whereas it is inconsistent with Fanning and Weaver (1997), whose baroclinic term is dominant. However, the model the latter group employed is an idealized atmospheric model consisting of energy and moisture conservation equations coupled to an idealized basin ocean general circulation model. The coupled system is then only driven by the prescribed incoming solar radiation at the top of the atmosphere along with an idealized zonal wind stress. Thus, the difference may be primary ascribed to the idealized zonal external forcing, which may have resulted in the weak east-west temperature gradient.

5.2 *The thermal response to changes in the Indo-Pacific circulation*

The structures of temperature and salinity are controlled by both the local buoyancy fluxes and advections. Therefore, the changes in the circulation can influence the structures of temperature and salinity to some extent.

The shading in Fig. 6 is the depth-latitude section of the temperature along 150°W. The SEC and NECC match the thermocline (20°C isotherm) between 3°S and 3°N and between 5°N and 10°N, respectively, since the geostrophic balance is held off the equator. The EUC matches the trough below the thermocline on the equator. Consistent with the intensified circulation, the meridional temperature gradients in LICOM are larger than that in L30T63. The ridge of the thermocline in LICOM is also sharper. Similar results for the eddy-resolving model were obtained by SC92 (their Fig. 5). The simulated temperatures by both models are generally cooler than the observed, especially in LICOM, due to the enhancement of the upwelling. As a result of the application of Richardson-number dependent vertical mixing (Pacanowski and Philander, 1981), a cool bias mainly exists beyond the thermocline, while the thermocline itself remains rather convergent.

As pointed out in section 4.3, there is a larger proportion of ITF transport confined in the upper layer in LICOM than in L30T63, which partly accounts for the difference of upper layer temperature in the Indian Ocean between the two models. The differences of SST between the two models are obscure since the restoring boundary condition is used (Fig. 10a). The warmer temperature produced by LICOM is mostly around Australia and off the southern cape of Africa. The differences in the subsurface (137.5 m) are distinct (Fig. 10b). There is a belt of warm water crossing the Indian Ocean from the exit of the ITF to Madagascar, flowing southward and round the Cape of Good Hope and finally extending to the Atlantic. The warm anomaly in the subsurface in LICOM also suggests a deeper thermocline along the route. The route follows

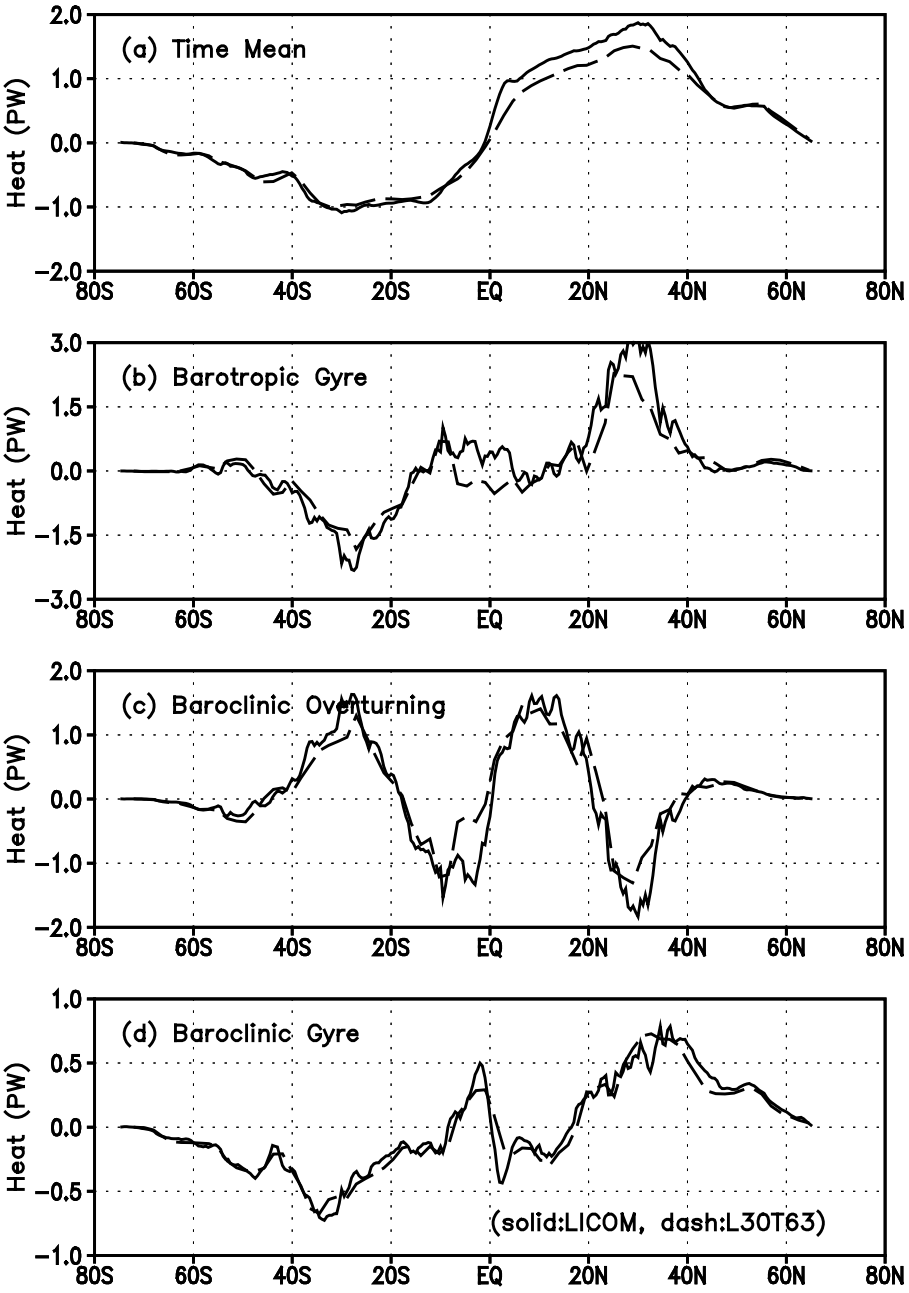

Fig. 9. The time mean (a), barotropic gyre (b), baroclinic overturning (c) and baroclinic gyre (d) components of the poleward heat transport for the global ocean simulated by LICOM (solid) and L30T63 (dashed) (units: PW).

the warm path of the global thermohaline circulation that was assumed by Gordon (1986).

There are two other patches of large positive temperature anomalies at the subsurface. One is at the south end of Africa and the other is near the southeast coast of Australia. The amplitudes of both anomalies exceed 4°C.

The upper layer circulation varies accordingly (figure not shown). For instance, the SEC of the Indian Ocean between 5°S and 15°S is enhanced in LICOM, which corresponds with the thermocline deepening in LICOM between 10°S and 20°S.

6. Conclusion and discussion

In the present study, an eddy-permitting quasi-global model, LICOM, with a uniform grid of 0.5° ×

0.5° was established based on the previous medium resolution model, L30T63. Forced by wind stresses from Hellerman and Rosenstain (1983), a 40-yr integration was conducted with SST and SSS being restored to the Levitus 94 dataset. The annual mean climatology of the LICOM control run is evaluated by the observation. A comparison between the LICOM control run and a parallel integration of L30T63, which has the same framework but a coarse resolution, was also made to confirm the impact of resolution on the model performance.

(1) The large-scale circulation can be well reproduced by LICOM. The transports of Kuroshio and the Gulf Stream exceed 60 Sv and 40 Sv, respectively. The intensity is 130 Sv for AAC and 16 Sv for NADW. All of the values agree with the simulation of SC92. On account of the reduction of horizontal viscosity with the enhancement of the horizontal resolution, the large scale circulations in LICOM are generally stronger than those in L30T63, especially the western boundary currents, ACC, Ekman cells around the equator, and the Deacon Cell.

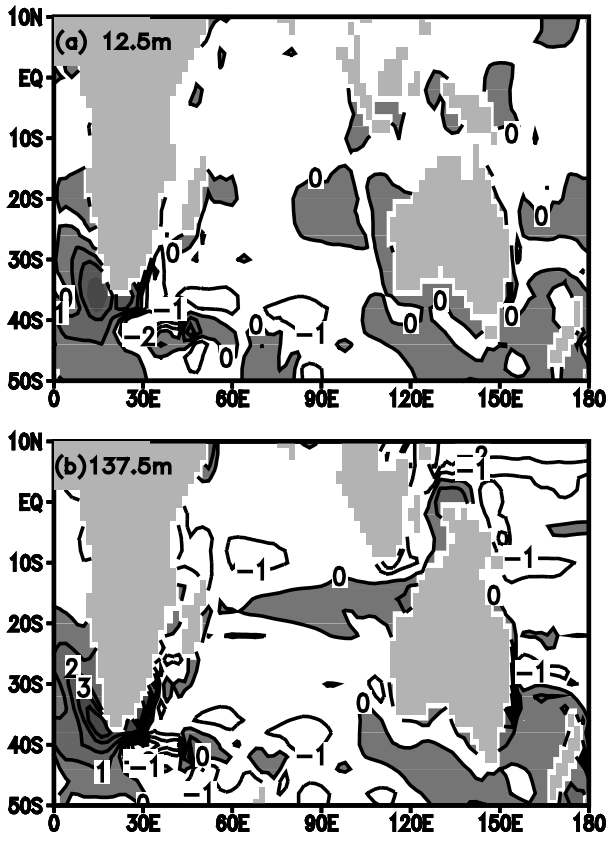

Fig. 10. The temperature differences (°C) between LICOM and L30T63 at the surface (a) and 137.5 m (b). Positive values are shaded, and the contours are at 0, 1, 2, 4, 6, and 8, respectively.

(2) The upper layer currents in the tropical Pacific are sensitive to both the horizontal resolution and the viscosity. In LICOM, the simulated EUC and SEC are greatly improved with respect to both the magnitude and structure. The temperature field also has a more realistic structure.

(3) LICOM yields an annual mean transport of 13.0 Sv for ITF. The Makassar Strait forms the main ITF passage within the Indonesian Sea, which agrees with the observation. There is, however, too much water exiting the Indonesian Seas through the Lombok Strait as soon as it outflows from the Makassar Strait. Compared with L30T63, the transport of ITF in LICOM is more convergent in the upper layer. As a consequence, the Indian Ocean tends to get warm in LICOM. A warm water band extending between 10°S and 20°S is evident in the Indian Ocean, especially in the subsurface layer.

(4) Due to the increase of time-mean large-scale circulation transports, the poleward heat transports for both the global and individual basins are significantly improved in LICOM. The decomposed analysis indicates that the transport due to the barotropic gyre, which primarily stands for the barotropic effect of the western boundary currents, is crucial in making the difference.

By intercomparing the simulations from seven tropical Pacific oceanic GCMs, Stockdale et al. (1993) propounded that to attain a realistic upper layer circulation in the tropical Pacific, it is essential to enhance the horizontal resolution and accordingly decrease the viscosity. The improvement of the tropical Pacific circulation in LICOM confirms this point of view. Another advantage from enhancing the horizontal resolution lies in the improved model ability to resolve the wave guide along the equator, which is beyond the scope of this paper and needs to be further addressed.

Since the main islands and straits within the Indonesian Archipelago can be resolved by the LICOM topography, the problem emerges regarding the which route the ITF takes. In the first experiment, the majority of water enters the Indonesian Sea via the Karimata and Torres Straits, instead of the Makassar Strait, in LICOM. The ITF route cannot be reproduced reasonably until the Makassar Strait is widened and the Karimata and Toress Straits are filled manually. Great care must be taken in treating the model topography within the Indonesian Sea to obtain a realistic representation of ITF. It is also noticed that in the Indian Ocean, the largest differences of circulation and temperature between LICOM and L30T63 occur in the subsurface layer, and these differences are ascribed to the difference in the modeled ITFs, especially the increased upper layer transport in LICOM.

New problems arise from increasing the model grid number. First of all, the computational cost is much higher for a long-term integration of a fine resolution model. This problem will not be solved until an efficient parallel algorithm and/or high performance parallel supercomputers are employed. Secondly, in the spherical coordinate system and with fine grid size, the convergence of meridians at high latitudes limits the timestep badly. Compromises include discarding the Arctic Ocean (as LICOM did in the present study) and moving the north pole to the land using a coordinate transform. An effort to adopt a reduced grid scheme (Wichett et al., 2000) in LICOM is being made by Liu et al. (2003), in which the Atlantic Ocean is included, making LICOM a global model.

Generally speaking, enhancement of the horizontal resolution decreases the dependence on the sub-grid parameterization and allows for a more faithful representation of ocean geometry and fine current structures (Griffies et al., 2000). But the issue is not always as simple as the theory suggests. Often, the results are model dependent. Based on the performance of LICOM, the annual mean circulation and temperature structures are improved, especially in the tropical and western boundary regions. Further research is needed to evaluate the seasonal and interannual variability in the model.

Acknowledgments. This work was jointly supported by the Chinese Academy of Sciences "Innovation Program" (Grant No. ZKCX2-SW-210), the National Key Program for Developing Basic Sciences (Grant G1999043808 and G2000078502), and the National Natural Science Foundation of China under Grant Nos. 40233031 and 40231004.

REFERENCES

Byan, F. O., and R. D. Smith, 1998: Modeling the North Atlantic circulation, from eddy-permitting to eddy-resolving. *International WOCE Newsletter*, **33**, 12–14.

Chen Keming, Zhang Xuehong, and Jin Xiangze, 1994: A coupled ocean-atmosphere general circulation model for studies of global climate changes, I. Formulation and performance of the model. *Acta Oceanologia Sinica*, **19**, 21–32. (in Chinese)

Covey, C., 1995: Global ocean circulation and equator-pole heat transport as a function of ocean GCM resolution, *Climate Dyn.*, **11**, 425–437.

Da Silva, A. M., C. C. Young, and S. Levitus, 1994: Atlas of surface marine data 1994, Vol.1: Algorithms and Procedures. NOAA Atlas NECDIS 6, U. S. Dept. of Commerce, Washington, DC, 83pp.

Dong Min, and Coauthors, 2000: The development and application of an atmospheric general circulation model for seasonal prediction. *Research on the short term climate prediction system in China*, Vol. 2, Beijing, China Meteorological Press, 63–69. (in Chinese)

Fang Guohong, Wei Zexun, Huang Qizhou, and Fang Wendong, 2002: Volume, heat and salt transports between the southern South China Sea and its adjacent waters, and their contribution to the Indonesian Throughflow. *Oceanologia et Limnologia Sinica*, **33**, 296–302. (in Chinese)

Fanning, A. F., and A. J. Weaver, 1997: A horizontal resolution and parameter sensitivity study of heat transport in an idealized coupled climate model, *J. Climate*, **10**, 2469–2478.

Fu, L. L., and R. D. Smith, 1996, Global ocean circulation from satellite altimetry and high-resolution computer simulation, *Bull. Amer. Meteor. Soc.*, **11**, 2625–2636.

Ganachaud, A., and C. Wunsch, 2003, Large-scale ocean heat and freshwater transports during the World Ocean Circulation Experiment. *J. Climate*, **16**, 696–705.

Gates, W. L., J. F. B. Mitchell, G. J. Boer, U. Cubasch, and V. P. Meleshlo, 1992: Climate modeling, climate prediction and model validation. *Climate Change, The Supplementary Report to the IPCC Scientific Assessment*, J. T. Honghton et al., Eds., Cambridge University Press, UK, 97–134.

Gent, P. R., and J. C. McWilliams, 1990: Isopycnal mixing in ocean circulation models. *J. Phys. Oceanogr.*, **20**, 150–155.

Gent, P. R., F. Bryan, S. Doney, and W. Large, 1999: A perspective on the ocean component of climate models. *CLIVAR Exchanges*, **4**, 11–14.

Godfrey, J. S., 1989: A Sverdrup model of the depth-integrated flow for the World Ocean, allowing for island circulations. *Geophys. Astrophys. Fluid Dyn.,* **45**, 89–112.

Godfrey, J. S., 1996: The effect of the Indonesian throughflow on ocean circulation and heat exchange with the atmosphere: A review. *J. Geophys. Res.*, **101**, 12217–12237.

Gordon, A. L., and J. L. McClean, 1999: Thermohaline stratification of the Indonesian Seas: Model and Observations, *J. Phys. Oceanogr.*, **29**, 198–216.

Gordon, A. L., R. D. Susanto, and A.L. Ffield, 1999: Throughflow within Makassar Strait. *Geophys. Res. Lett.,* **26**, 3325–3328.

Gordon, A., 1986, Interocean exchange of thermocline water. *J. Geophys. Res.*, **91**, 5037–5046.

Griffies, S. M., and coauthors, 2000: Development in ocean climate modeling. *Ocean Modeling*, **2**, 123–192.

Haney, R. L., 1971: Surface thermal boundary conditions for ocean circulation models. *J. Phys. Oceanogr.*, **1**, 241–248.

Hellerman, S., and M. Rosenstein, 1983: Normal monthly wind stress over the world ocean with error estimates. *J. Phys. Oceanagr.*, **13**, 1093–1104.

Hirst, A. C., and J. S. Godfrey, 1993: The role of the Indonesian Throughflow in a global GCM. *J. Phys. Oceanogr.*, **23**, 1057–1086.

IPCC, 2001: *Climate Change 2001: The Scientific Basis*, Contribution of Working Group I to the Third Assessment Report of the Intergovernmental Panel on Climate Change (IPCC), J. T. Houghton et al., Eds., Cambridge University Press, UK, 944pp.

Jin Xiangze, Zhang Xuehong, and Zhou Tianjun, 1999: Fundamental framework and experiments of the third generation of IAP/LASG world ocean general circulation model. *Adv. Atmos. Sci.*, **16**, 197–215.

Jin Xiangze, Yu Yongqiang, Zhang Xuehong, Zhou Tianjun, and Liu Hailong, 2000: The simulated wind driven circulation and thermohaline circulation by L30T63 oceanic general circulation model. *Research on the Short Term Climate Prediction System in China*, Vol.2, China Meteorological Press, Beijing. (in Chinese)

Kiehl, J. F., J. J. Hack, G. B. Bonan, B. A. Boville, D. L. Willianmson, and P. J. Pasch, 1998: The National Center for Atmospheric Research Community Climate Model: CCM3. *J. Clim.*, **11**, 1131–1149.

Lebdev, K. V., and M. I. Yaremchuk, 2000: A diagnostic study of the Indonesian Throughflow. *J. Geophys. Res.,* **105**, 11243–11258.

Levitus, S., and T. P. Boyer, 1994: World Ocean Atlas 1994 Volume 4: Temperature. NOAA Atlas NESDIS 4. U. S. Department of Commerce, Washington, D. C. 117pp.

Levitus, S., R. Burgett, and T. P. Boyer, 1994: World Ocean Atlas 1994 Volume 3: Salinity. NOAA Atlas NESDIS 3., U. S. Department of Commerce, Washington, D. C. 99pp.

Liu Hailong, 2002: High resolution oceanic general circulation model and the simulation of the upper ocean circulation in the tropical Pacific. Ph.D. dissertation, Graduate School of the Chinese Academy of Sciences, 178pp. (in Chinese)

Liu Hui, Jin Xiangze, Zhang Xuehong, and Wu Guoxiong, 1996: A coupling experiment of an atmosphere and an ocean model with a monthly anomaly exchange scheme. *Adv. Atmos. Sci.*, **13**, 133–146.

Liu Xiying, 2001: The simulation and study of sea-ice-air interaction in the northern high latitude region, Ph.D. dissertation, Graduate School of the Chinese Academy of Sciences, 136pp. (in Chinese)

Liu Xiying, Liu Hailong, Zhang Xuehong, and Yu Rucong, 2003: Implementation of a reduced grid in IAP/LASG world ocean general circulation models. LASG Report No. 10, March, 2003, 8–20.

Liu Xiying, Zhang Xuehong, Yu Yongqiang, and Yu Rucong, 2004: Mean climatic characteristics in high northern latitudes in an ocean-sea ice-atmosphere coupled model. *Adv. Atmos. Sci.*, **21**, 236–244.

Masumoto, Y., and T. Yamagata, 1996: Seasonal variations of the Indonesian throughflow in a general circulation model, *J. Geophys. Res.*, **101**, 12287–12294.

Molcard, R., M. Fieux, and A.G. Ilahude, 1996: The Indo-Pacific throughflow in the Timor Passage. *J. Geophys. Res.,* **101**, 12411–12420.

Molcard, R., M. Fieux, and F. Syamsudinb, 2001: The throughflow within Ombai Strait. *Deep-Sea Res.,* **48,** 1237–1253.

Murray, S. P., and D. Arief, 1988: Throughflow into the Indian Ocean through Lombok Strait, January 1985-January 1986. *Nature*, **333**, 444–447.

Pacanowski, R. C., and S. G. H. Philander, 1981: Parameterization of vertical mixing in numerical models of the tropical ocean. *J. Phys. Oceanagr.*, **11**, 1442–1451.

Pacanowski, R., 1995: MOM 2 Documentation: Users Guide and Reference Manual ver 1.0. GFDL Ocean Group Technical Report No. 3, NOAA/Geophysical Fluid Dynamics Laboratory, Princeton, NJ, 232pp.

Philander, S. G. H., 1990: *El Niño, La Niña, and the Southern Oscillation.* Academic Press, 293pp.

Schneider, N., 1998: The Indonesian Throughflow and the global climate system. *J. Clim.*, **11**, 676–689.

Schneider, N., and T. P. Barnett, 1997: Indonesian Throughflow in a CGCM. *J. Geophys. Res.*, **102**, 12341–12358.

Semtner, A. J., and R. M. Chervin, 1988: A simulation of the global ocean circulation with resolved eddies. *J. Geophys. Res.*, **93**, 15502–15522.

Semtner, A. J., and R. M. Chervin, 1992: Ocean general circulation from a global eddy-resolving model. *J. Geophys. Res.*, **97**, 5493–5550.

Smith, R. D., J. K. Dukowicz, and R. C. Malone, 1992: Parallel Ocean General Circulation Modeling. *Physica D*, **60**, 38–61.

Stammer, D., R. Tokmakian, A. Semtner, and C. Wunsch, 1996, How well does a (1/4)° global circulation model simulate large-scale oceanic observations. *J. Geophys. Res.*, **101**, 25779–25811.

Stockdale, T., D. Anderson, M. Davey, P. Delecluse, A. Katternburg, Y. Kitamura, M. Latif, and T. Yamagata, 1993: Intercomparison of tropical ocean GCMs. *Tech. Doc. WMO.TD 545*, 43pp.

Wajsowicz, R. C., and E. K. Schneider, 2001: The Indonesian Throughflow's effect on global climate determined from the COLA coupled climate system. *J. Climate*, **14**, 3029–3042.

Wei Zexun, 1999: Diagnostic study of the world ocean and North Pacific circulation. M. S. thesis, Institute of Oceanography, Chinese Academy of Sciences, 37pp. (in Chinese)

Whitworth, T. III, 1983: Monitoring the transport of the Antarctic Circumpolar Current at Drake Passage. *J. Phys. Oceanogr.*, **13**, 2045–2057.

Wickett, M. E., P. B. Duffy, and G. Rodriguez, 2000: A reduced grid for a parallel global ocean general circulation model. *Ocean Modelling*, **2**, 85–107.

Wolanski, E., E. Rido, and M. Inoue, 1988: Currents through Torres. *J. Phys. Oceanogr.*, **18**, 1535–1545.

Wu Guoxiong, Liu Hui, Zhao Yuncheng, and Li Weiping, 1996: A nine-layer atmospheric general circulation model and its performance. *Adv. Atmos. Sci.*, **13**, 1–18.

Wu Guoxiong, and Coauthors, 1997: Global ocean-atmosphere-land system model of LASG (GOALS/LASG) and its performance in simulation study. *Quart. J. Appl. Meteor.* (Suppl.), 15–28. (in Chinese)

Wunsch, W., 1996: *The Ocean Circulation Inverse Problem*, Cambridge University Press, 442pp.

Yu Yongqiang, 1997: Design of ocean-atmosphere-sea ice coupling scheme and simulation of interdecadal oscillation of climate. Ph. D. dissertation, Institute of Atmospheric Physics, Chinese Academy of Sciences, 130pp. (in Chinese)

Yu Yongqiang, and Zhang Xuehong, 1998: A modified air-sea flux anomaly coupling scheme. *Chinese Science Bulletin*, **43**, 866–870. (in Chinese)

Yu Yongqiang, Zhang Xuehong, Jin Xiangze, and Zhou Tianjun, 2000: The air-sea flux anomaly coupling scheme. *Research on the Short Term Climate Prediction System in China*, **2**, China Meteorological Press, Beijing, 201–207.

Yu Yongqiang, Yu Rucong, Zhang Xuehong, and Liu Hailong, 2002: A flexible coupled ocean-atmosphere general circulation model. *Adv. Atmos. Sci.*, **19**, 169–190.

Zhang Xuehong, and Liang Xinzhong, 1989: A numerical world ocean general circulation model. *Adv. Atmos. Sci.*, **6**, 43–61.

Zhang Xuehong, Bao Ning, Yu Rucong, and Wang Wanqiu, 1992: Coupling scheme experiments based on an atmospheric and an oceanic GCM. *Chinese J. Atmos. Sci.*, **16**, 129–144.

Zhang Xuehong, Chen Keming, Jin Xiangze, Lin Wuyin, and Yu Yongqiang, 1996: Simulation of the thermohaline circulation with a twenty-layer oceanic general circulation model. *Theoretical and Applied Climatology*, **55**, 65–87.

Zeng Qingcun, Zhang Xuehong, Liang Xinzhong, Yuan Chongguang, and Chen Shengfang, 1989: Documentation of IAP two-level Atmospheric General Circulation Model. DOE/ER/60314-H1, TR044, 383pp.